*J. Biochem.* **140**, 375–381 (2006)
doi:10.1093/jb/mvj164

# Crystal Structures of the *Nicotiana glutinosa* Ribonuclease NT in Complex with Nucleoside Monophosphates

**Shin Kawano, Yoshimitsu Kakuta, Takashi Nakashima and Makoto Kimura***
*Laboratory of Biochemistry, Department of Bioscience and Biotechnology, Faculty of Agriculture, Graduate School, Kyushu University, Hakozaki 6-10-1, Higashi-ku, Fukuoka 812-8581*

Received May 1, 2006; accepted July 11, 2006

**Ribonuclease NT (RNase NT), induced upon tobacco mosaic virus (TMV) infection in *Nicotiana glutinosa* leaves, has a broad base specificity. The crystal structures of RNase NT in complex with either 5′-AMP, 5′-GMP, or 2′-UMP were determined at 1.8 Å resolutions by molecular replacement. RNase NT consists of seven helices and seven β strands, and the structure is highly similar to that of RNase NW, a guanylic acid preferential RNase from the *N. glutinosa* leaves, showing root mean square deviation (rmsd) of 1.1 Å over an entire length of two molecules for Cα atoms. The complex structures revealed that Trp42, Asn44, and Trp50 are involved in interactions with bases at B1 site (primary site), whereas Gln12, Tyr17, Ser78, Leu79, and Phe89 participate in recognition of bases at B2 site (subsite). The 5′-GMP and 5′-AMP bind both B1 and B2 sites in RNase NT, while 2′-UMP predominantly binds B1 site in the complex. The nucleotide binding modes in these complexes would provide a clue to elucidation of structural basis for the broad base specificity for RNase NT.**

**Key words: base specificity, crystal structure, *Nicotiana glutinosa*, nucleotide binding, RNase.**

Abbreviations: AMP, monophosphate adenylic acid; GMP, monophosphate guanylic acid; UMP, monophosphate uridylic acid; ApA, adenylyl-3′,5′-adenosine; GpG, guanylyl-3′,5′-guanosine; Poly A, polyadenylic acid; Poly I, polyinosinic acid; Poly U, polyuridylic acid; rmsd, root mean square deviation; RNase, ribonuclease; RNase NT, TMV-inducible RNase from *N. glutinosa*; rRNase NT, recombinant RNase NT; TMV, tobacco mosaic virus.

Ribonucleases (RNases), belonging to the RNase T2 family, are ubiquitous from viruses to human cells and implicated in diverse functions in organisms (*1*). They are single polypeptide chains with about 200 amino acid residues and contain two common sequences CAS I and CAS II with two invariant histidine residues that are crucial for catalytic activity (*1*). The best characterized enzyme of the RNase T2 family is RNase Rh from *Rhizopus niveus* (*2*). RNase Rh comprises 222 amino acid residues with five disulfide bonds (*2*). The adenylic preference (A>G>U,C) of RNase Rh was estimated based on the release of nucleotides from RNA during the course of hydrolysis (*3*). Kinetic and site-directed mutagenesis studies identified His46, His109, His104, Glu105, and Lys108 as catalytic amino acid residues; the former two histidine residues function as general acid and base catalysis in the transfer reaction (*4*, *5* and references therein). The crystal structure of RNase Rh in a complex with 2′-AMP revealed that Trp49, Asp51, and Tyr57 are involved in interactions with the adenosine base (*6*, *7*).

Since McClure *et al*. discovered that the *S*-glycoproteins associated with gametophytic self-incompatibility in the Solanaceae have ribonuclease activity (*8*), a large amount of sequence information has been available for plant RNases (*9*). On the basis of sequence comparison, plant RNases are classified into the RNase T2 family. Subsequently, enzymatic properties were examined on plant RNases (*10*–*12*) and these studies revealed that they are classified into two groups in terms of substrate preference: the tomato type is G>A>U>C, and the seed type is U>G>A,C (*12*). To understand structural basis for substrate preference of plant RNases, we earlier determined crystal structures of the seed type: uridine-preferential bitter gourd RNase MC1 (*13*, *14*) and the tomato type: guanosine-preferential RNase NW from the *Nicotiana glutinosa* leaves (*15*). These results, together with results obtained by biochemical studies, elucidated structural basis for their base preference at an atomic level (*15*, *16*).

In the course of study of RNase NW from *N. glutinosa* leaves, a distinct cDNA encoding RNase NT (formerly designated as RNase NGR3) specifically induced upon TMV-infection was found (*17*). Subsequent expression in *Escherichia coli* cells and characterization of the recombinant enzyme indicated that RNase NT cleaved homopolynucleotides, Poly A, Poly I, and Poly U, at a comparable rate (*18*). This result indicated that RNase NT seemed to be distinct from other plant RNases classified into tomato- and seed-types, including RNase NW and RNase MC1, respectively.

In order to gain further insight into the structural basis for base specificity of plant RNases, we attempted to crystallize RNase NT in complex with nucleoside monophosphates, and the crystals complexed with 5′-GMP, 5′-AMP, or 2′-UMP grew under an appropriate condition. In the present study, we have analyzed their crystal structures in the expectation that this will be help in establishing structural basis for a broad substrate specificity

*To whom corresponding should be addressed. Tel/Fax: +81-92-642-2853, E-mail: mkimura@agr.kyushu-u.ac.jp

 

of RNase NT. In this paper, we described the crystal structures of RNase NT complexed with either 5′-GMP, 5′-AMP, or 2′-UMP and discussed the structural basis for the broad base specificity of RNase NT, comparing with that of a guanylic acid preferential RNase NW.

## MATERIALS AND METHODS

*Materials*—The cDNA encoding RNase NT was previously cloned and sequenced (*17*). Multi-Copy Pichia Expression kits, including the expression plasmid pPIC9K and host strain GS115 were obtained from Invitrogen. DNA modification enzymes were obtained from MBI Fermentas. Amicon Ultra used for concentration for the protein was obtained from Millipore. The oligonucleotide primers and plasmid pGEM T-vector were purchased from Amersham Pharmacia Biotech. All nucleoside monophosphates were purchased from Sigma Chemical Co. All other reagents and chemicals were of analytical grade.

*Expression and Purification of rRNase NT*—The cDNA fragment with artificial recognition sites of *Eco*RI and *Not*I at 5′- and 3′-ends, respectively, was amplified by PCR from the RNase NT cDNA, using sense: GAATTCGCACAG-GACTTTGATTTCTTCTAC and anti-sense: GCGGCCGC-TTAAAATTCATCATTGGTCAGAC primers (nucleotides underlined indicate recognition sites by *Eco*RI and *Not*I, respectively), and the resulting product was first ligated to the pGEM T-vector, by which the *E. coli* cell JM109 was transformed. Since the cloned RNase NT cDNA contains an *Eco*RI and a *Bgl*II recognition sites, the internal C residues (positions 196 and 603) were replaced with T by site-directed mutagenesis to avoid restriction enzymatic scission. Expression of the RNase NT cDNA in *Pichia pastoris* and purification of the resulting protein (rRNase NT) was done in the same manner as described for RNase NW (*15*).

*Crystallization*—The purified protein rRNase NT was concentrated to 11.2 mg/ml in water. Crystallization trials were made by the hanging-drop vapor diffusion method at 20°C using crystallization screen kits Crystal Screens I and II (Hampton Research) and Wizard I and II (Emerald BioStructures) as reservoir solutions. Crystals of rRNase NT were obtained within 2 days under conditions of 100 mM sodium acetate, pH 4.5, containing 20% (v/v) 1,4-butanediol (Wizard I, number 35). To obtain the complex crystals, the protein crystals were crushed and seeded into the solution containing rRNase NT (11.2 mg/ml) and nucleoside monophosphates (1–10 mM), such as 2′-GMP, 3′-GMP, 5′-GMP, 2′-AMP, 3′-AMP, 5′-AMP, 2′-UMP, 3′-UMP, or 5′-UMP. The complex crystals used for data collection were finally obtained from a drop of 2 μl of rRNase NT and 1 μl of either 2 mM 5′-GMP, 5 mM 5′-AMP, or 5 mM 2′-UMP.

*Data Collection and Processing*—The crystals were soaked stepwise from 25 to 30% (v/v) 1,4-butanediol in the reservoir solution for a few minutes, suspended on a loop in a thin liquid film of stabilizing solution, and directly frozen at 100 K in a cold nitrogen gas stream with a Cryostream Cooler. Diffraction data were collected using an oscillation method at 100 K on ADSC Quantum 4R CCD detector at beamline BL38B1, BL40B2, and MAR CCD detector at BL44B2 of SPring-8, Japan. Diffraction images were processed and scaled with HKL2000 (*19*). All crystals were orthrombic with space group $P2_12_12_1$, and unit cell dimensions of three complexes were almost identical (Table 1).

Table 1. **Data collections and refinement statistics of RNase NT complexed with substrate analogues.**

| | | | |
|---|---|---|---|
| Data collections | | | |
| Data set | 5′-GMP | 5′-AMP | 2′-UMP |
| Beam line | BL40B2 | BL38B1 | BL38B1 |
| Space group | $P2_12_12_1$ | $P2_12_12_1$ | $P2_12_12_1$ |
| Unit cell dimension | 37.28 Å | 37.289 Å | 37.272 Å |
| | 69.547 Å | 69.787 Å | 68.984 Å |
| | 73.969 Å | 73.748 Å | 73.863 Å |
| Resolution (Å) | 20–1.8 | 20–1.8 | 20–1.8 |
| Wavelength (Å) | 0.9 | 0.9 | 0.9 |
| Multiplicity | 8.7 | 7.0 | 5.5 |
| $I/\sigma$ $(I)^a$ | 23.9 (24.6) | 23.0 (28.8) | 36.2 (4.2) |
| Completeness (%)[a] | 99.0 (98.8) | 99.7 (100) | 96.2 (69.2) |
| $R_{sym}$ [a,b] | 4.5 (23.6) | 4.0 (19.6) | 5.2 (27.6) |
| Refinement | | | |
| $R_{work}/R_{free}$ (%)[c] | 21.7/25.2 | 22.1/25.6 | 20.9/25.1 |
| Bond length (Å) | 0.009 | 0.005 | 0.005 |
| Bond angles (deg.) | 1.6 | 1.4 | 1.4 |
| Ramachandran plot | | | |
| Most favored regions (%) | 87.5 | 86.9 | 88.1 |
| Additional allowed regions (%) | 11.9 | 11.9 | 11.9 |
| Generously allowed regions (%) | 0.6 | 1.1 | 0 |
| <Number of observed substrate analogue(s)> | 2 | 2 | 1 |

[a]Values in parentheses correspond to the highest resolution shell. [b]$R_{sym} = \Sigma|I_i - \langle I\rangle|/\Sigma I_i$, where $I_i$ is the intensity of the $i$th observation and $\langle I\rangle$ is the mean intensity of the reflection. [c]$R_{free}$ was calculated with 5% of the data omitted from structure refinement.

*Structure Determination and Refinement*—The structures of rRNase NT in complex with nucleoside monophosphates were determined using the molecular replacement method with CNS (*20*). The structure of RNase NW (PDB code, 1IYB), which shares 47% identical amino acid residues with RNase NT, served as a search model. After protein atoms were refined by simulated annealing, the relative positions of each nucleoside monophosphate were unambiguously determined based on difference electron density. Refinement against 1.8 Å data was done using CNS with rounds of manual rebuilding in O (*21*). The stereochemical checks were carried out using PROCHECK (*22*). Data collection and refinement statistics were given in Table 1. The atomic coordinates of the complexes rRNase NT–5′-GMP, rRNase NT–5′-AMP, and rRNase NT–2′-UMP have been deposited in the Protein Data Bank under the accession codes 1VCZ, 1VD1, and 1VD3, respectively.

*Nomenclature for Substrate Binding Sites*—RNases have the primary site and subsite for bases located at 5′- and 3′-terminal ends of a scissile bond, respectively. In this report, the primary site and subsite were referred to as B1 and B2 sites, respectively, according to the nomenclature by Allewell and Wyckoff (*23*).

## RESULTS AND DISCUSSION

*Structure Determination*—We previously constructed the *E. coli* expression system for RNase NT using pET-22b as an expression plasmid (*18*). In this system, the recombinant RNase NT could be secreted into the *E. coli* periplasmic space with the aid of the *pelB* signal sequence and characterized in terms of enzymatic properties (*18*). However, the yields were extremely low: less than 0.1 mg protein per liter of cultured cells. Hence, we attempted to express the cDNA encoding RNase NT in *P. pastoris*, using the expression plasmid pPIC9K, as described for that of the cDNA encoding RNase NW. The purified rRNase NT gave a single band on SDS-PAGE (data not shown). The direct N-terminal sequencing provided a single sequence: Tyr-Val-Glu-Phe-Ala-Gln. This result indicated a cleavage by the STE13 gene product at the peptide bond between Ala and Tyr in the α-factor signal sequence, giving rise to rRNase NT which has an extra four amino acid sequence (Tyr-Val-Glu-Phe) attached to the N-terminal amino acid residue of RNase NT.

Since no crystals of rRNase NT in complex with nucleoside monophosphates grew under any conditions used, the rRNase NT crystals were first obtained under conditions described above. Then, crystals of the complex rRNase NT-nucleoside monophosphates successfully grew by seeding the rRNase NT crystals into the protein solution containing either 5′-GMP (2 mM), 5′-AMP (5 mM), or 2′-UMP (5 mM). The crystals of the three complexes belong to space group $P2_12_12_1$ with one molecule in the crystallographic asymmetric unit. The statistics of data collection are summarized in Table 1. The crystal structures of rRNase NT complexed with either 5′-GMP, 5′-AMP, or 2′-UMP were determined from electron density maps that were phased using the RNase NW structure (*15*) as a search model, as described under Materials and Methods. The phasings provided clear electron density maps for an entire length of the protein and the crystal structures are well ordered except only three residues (Gly192–Gly194) disordered in the complex structure with 5′-GMP. After several rounds of refinement and manual fitting, the rRNase NT structures in complex with 5′-GMP, 5′-AMP, and 2′-UMP were refined to the $R_{work}/R_{free}$ values of 22%/25%, 22%/26%, and 21%/25%, respectively. The electron densities for 5′-GMP, 5′-AMP, and 2′-UMP bound to rRNase NT were clearly seen in the three complexes; the electron density for 5′-AMP bound at the B1 and B2 sites in rRNase NT are representatively shown in Fig. 1. The models have geometries close to ideal with rmsd values of between 0.005 Å and 0.009 Å and between 1.4° and 1.6° from ideal values for bond lengths and angles, respectively. When the structures were checked using PROCHECK (*22*), 86.9–88.1% of the non-glycine and non-proline residues fell in the most favored regions and 11.9% in the additional allowed regions of the Ramachandran plot. The final electron density maps were of high quality but a few of residues at N- and C-terminal were not determined. The structures were finally refined at 1.8 Å resolution and refinement statistics were shown in Table 1.

*Overall Structure*—The crystal structure of rRNase NT in complex with 5′-AMP is representatively shown in Fig. 2. Secondary structure elements of RNase NT, as defined by the PROCHECK (*22*), and sequence alignment

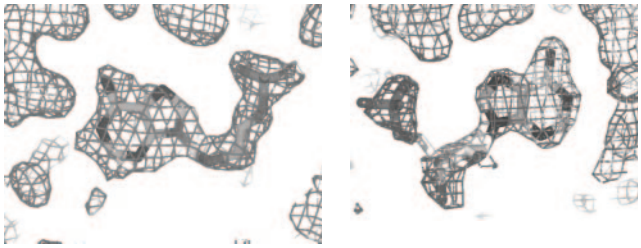


Fig. 1. **Composite omit maps for 5′-AMP bound rRNase NT.** The composite annealed omit maps ($2F_0 - F_c$) were calculated, and the electron density is contoured at 1.2 σ level.

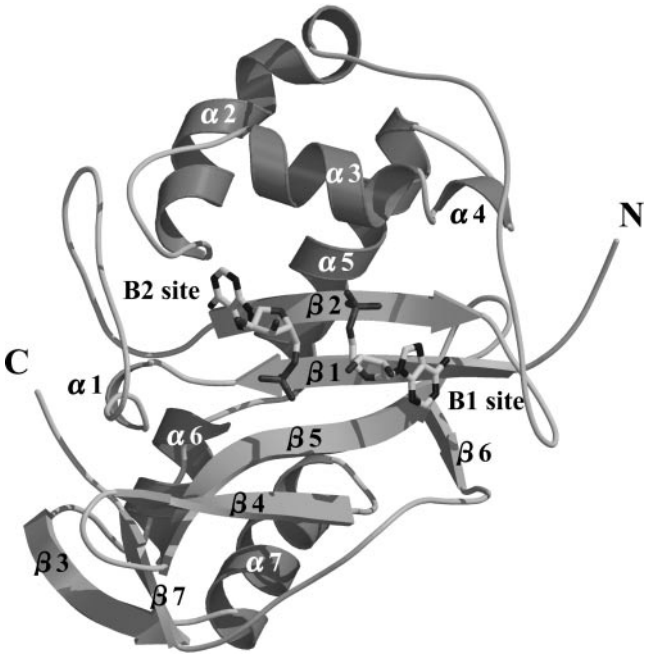


Fig. 2. **Ribbon representation of crystal structure of rRNase NT complexed with 5′-AMP.** RNase NT structurally belongs to the α + β class of proteins, having seven helices and seven β-strands. Two 5′-AMP molecules observed at the B1 and B2 sites in the crystal structure of the complex rRNase NT–5′-AMP are indicated.

with RNase NW are given in Fig. 3. RNase NT is composed of seven helices (α1–α7) and seven β-strands (β1–β7), characteristic of the α + β type structure. The amino acid residues (β1: 6–12 and β2: 37–43) at the N-terminal region form a two-stranded antiparallel β-sheet, intervening one $3_{10}$ helix (α1: 14–16) and loop structures. The polypeptide enters the extended helical structures (α2: 62–75, α3: 87–95, α4: 98–100, α5: 105–119, and α6: 121–128), having a short β strand (β3: 133–139) followed by α-helix (α7: 140–151). The amino acid residues at the C-terminal region form an antiparallel β-sheet (β4: 156–162 and β5: 167–176), forming a central antiparallel pleated β-sheet with the N-terminal β-strands (β1-β3). The structure was completed by β-strands (β6: 183–185 and β7: 198–201) intervening a long loop structure. The overall structure of RNase NT has a significant similarity to those of other known plant RNases, such as RNase NW


Fig. 3. **Sequence comparison of RNase NT with that of RNase NW.** The secondary structure elements indicated are those defined using the program PROCHECK (*22*). α-helices and $3_{10}$-helices are indicated by bars. β-strands are indicated by arrows. NT and NW indicate RNase NT and RNase NW, respectively. Stars and pluses indicate amino acid residues assigned as amino acids to constitute the B1 and B2 sites, respectively in RNase NT and RNase NW.

from the *N. glutinosa* leaves (*15*) and RNase MC1 from the bitter gourd seeds (*13*). A structural superposition of Cα atoms over the entire RNase NT with RNase NW, determined using the program O, gave the rmsd value of 1.1 Å.

*5′-GMP Bound to RNase NT*—Two 5′-GMP molecules bind through an extensive hydrogen bond network and hydrophobic interactions (Fig. 4, A and B). The one molecule binds rRNase NT in a manner similar to 2′-AMP in the crystal structure of RNase Rh in complex with 2′-AMP (Fig. 4A) (*6*, *7*). Namely, Trp42, Asn44, and Trp50, which correspond to Trp49, Asp51, and Tyr57 assigned as amino acids to constitute the B1 site in RNase Rh, are involved in interaction with the guanine base, a finding which suggests an adequate binding of the guanine base of 5′-GMP to RNase NT. The orientation of Trp50 is in parallel to the guanine base at 3.6 Å distance and the indole ring of Trp42 covers the base at angle of 30° from 4.5 Å distance. The side chain amide oxygen atom of Asn44 makes hydrogen bond to the N1 atom (2.68 Å) of the guanine base (Fig. 4A).

The other 5′-GMP molecule binds the B2 site in a manner similar to 5′-GMP bound at the B2 site in guanylic acid preferential RNase NW (Fig. 4B). This finding again suggests an appropriate binding of the guanine base of 5′-GMP to RNase NT. In the complex, the guanine moiety of 5′-GMP is stabilized in a hydrophobic pocket *via* a sandwich-like stacking interaction with two aromatic side chains of Tyr17 and Phe89. The aromatic ring of Phe89 is oriented in parallel to the guanine base at 4.0 Å distance and that of Tyr17 covers the base at angle of 33° from 4.5 Å distance. In addition, the N7 atom and O6 atom are anchored to the hydroxyl group of the side chain of Ser78 (2.78 Å) and to the N atom of the main chain of Leu79 (2.73 Å), respectively (Fig. 4B). Only a slight distinct binding mode is that in the rRNase NT–5′-GMP complex, the N2 atom of the guanine base forms hydrogen bonding interactions *via* the structural water molecule (2.48 Å) to the side chain of Gln12 (2.81 Å) in RNase NT, while the N1 atom of the guanine base directly donates hydrogen bond to the side chain amide oxygen atom of Gln12 in the RNase NW–5′-GMP complex. This difference is probably due to a slight enlargement of the binding pocket caused by substitution of Thr78 in RNase NW with Ser78 in RNase NT.

*5′-AMP Bound to RNase NT*—Two molecules of 5′-AMP, like the case for 5′-GMP in the rRNase NT–5′-GMP complex, bind rRNase NT in the structure of the complex rRNase NT–5′-AMP (Fig. 4, C and D). As for 5′-AMP bound at B1 site, the adenine base is sandwiched by the indole rings of Trp42 and Trp50 and stabilized by a hydrogen bond of the side chain of Asn44 (2.81 Å). This binding mode suggests an adequate binding of the adenine base of 5′-AMP to RNase NT, though the orientation of the adenine base is distinct from that of the guanine base of 5′-GMP bound at the B1 site in RNase NT (Fig. 4A). The electron density for the phosphate group of 5′-AMP bound to the B1 site is well defined and allows a straightforward modeling of the phosphate group into its binding site, as shown in Fig. 4C. The imidazole groups of His97 as well as the neighboring His92 capture O atoms of the phosphate group (2.58 Å and 2.53 Å, respectively), cooperating with the side chain of Glu93 (2.72 Å).

Although the adenine base of 5′-AMP binds the B2 site (Fig 4D), it shows a different orientation from the guanine base of 5′-GMP (Fig 4B). Thus, the glycosyl torsion angle of 5′-AMP adopts an *anti* conformation (Fig. 4D), while that of 5′-GMP in the B2 site in RNase NT is a *syn* conformation (Fig. 4B). As a result, the N1 atom of the adenine ring interacts with the amide group of the main chain of Leu79 (2.92 Å), and the N6 and N7 atoms interact with Oε1 (2.79 Å) and Nε2 (2.92 Å) of the side chain of Gln12, respectively. In addition, Ser78 is not involved in interaction with the adenine base, though it hydrogen bonds to the guanine base in the complex rRNase NT–5′-GMP. Furthermore, it should be noted that the orientation of the Gln12 side chain in the complex rRNase NT–5′-AMP is slightly different from that in the complex rRNase NT–5′-GMP (Fig. 4, B and D), while the positions of amino acid residues of the B1 site are identical, irrespective of the base difference (Fig. 4, A and C). This finding suggests a more flexible recognition mode of the B2 site than that of the B1 site in RNase NT toward distinct bases.

*2′-UMP Bound to RNase NT*—In contrast to 5′-GMP and 5′-AMP in the complexes, 2′-UMP predominantly binds the B1 site in the crystal structure of the complex rRNase NT–2′-UMP (Fig. 4, E and F). Two distinct orientations of the side chain of Asn44 were observed; each side chain interacts with both O4 (3.10 Å) and N3 of the uracil base, intermediating with water molecules, by hydrogen bondings (Fig. 4, E and F). The conformer shown in Fig. 4E is the major conformer having an occupancy of 0.6 and an average *B*-factor of 10.6 $Å^2$. The minor conformer, as given in Fig. 4F, has an occupancy of 0.4 and an average *B*-factor of 24.9 $Å^2$. The uracil base is sandwiched by the hydrophobic indole rings of Trp50 and Trp42. The phosphate group is, as the cases for 5′-AMP, firmly

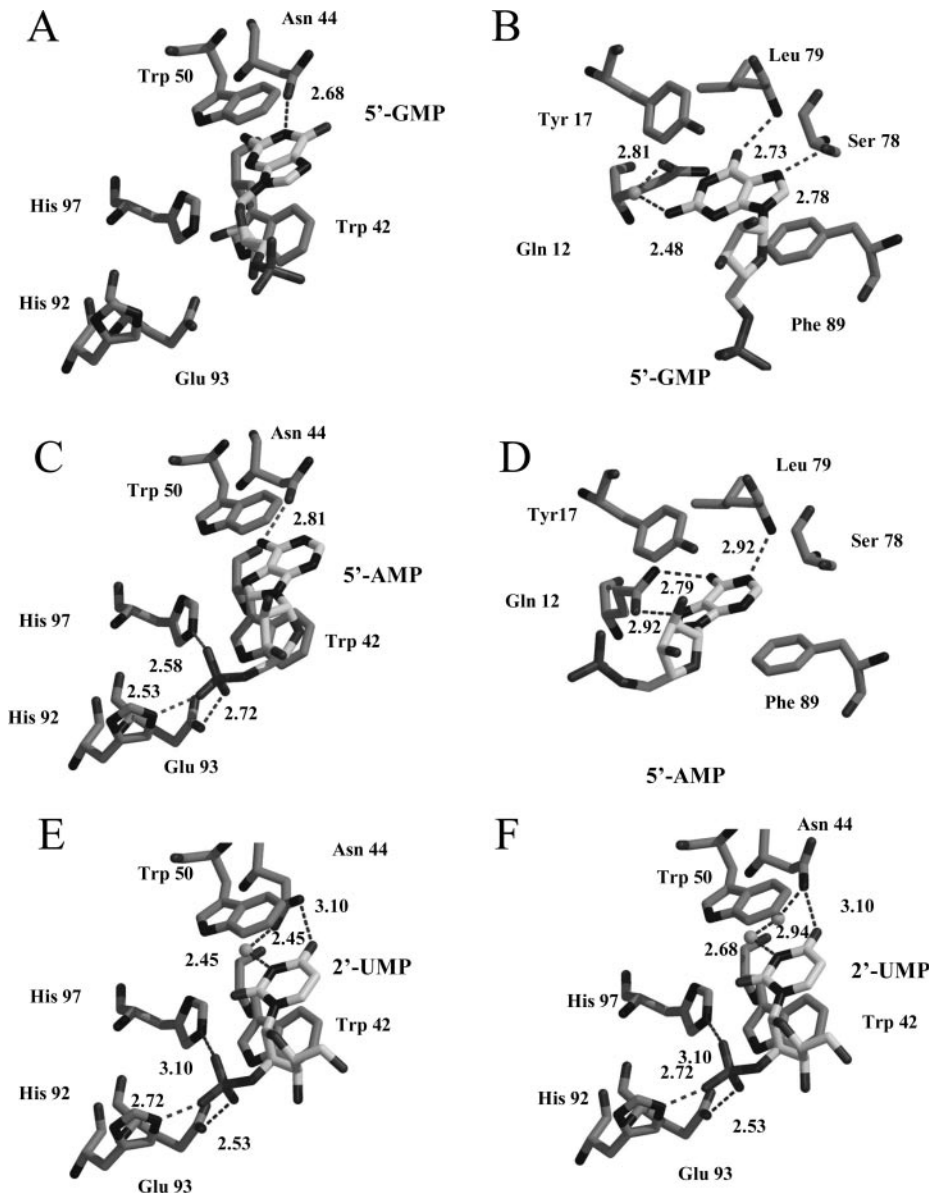


Fig. 4. **Conformations of amino acids composed of the B1 and B2 sites in RNase NT.** A, 5′-GMP binding at the B1 site. B, 5′-GMP binding at the B2 site. C, 5′-AMP binding at the B1 site. D, 5′-AMP binding at the B2 site. E and F, 2′-UMP binding at the B1 site, showing an alternative conformation of Asn44. Hydrogen bonds and distances (Å) between atoms and the others are shown by dash line and number, respectively. Water molecules are described as spheres. All distances are enough to make hydrogen bonding.

stabilized by hydrogen bonding interactions with the side chains of His92 (2.72 Å), Glu93 (2.53 Å), and His97 (3.10 Å).

## DISCUSSION

We previously isolated from *N. glutinosa* leaves two distinct cDNA clones, *NGR1* and *NGR3*, which were induced by a mechanical wounding and TMV-infection, respectively (*17*). Subsequently, both *NGR1* and *NGR3* were expressed in *E. coli* cells, and their translational products RNase NW and RNase NT, respectively, were characterized in terms of substrate specificity (*18*). The result indicated that RNase NW preferentially cleaved Poly I, while RNase NT hydrolyzed Poly A, Poly I, and Poly U at a comparable rate. It was thus concluded that RNase NW is a guanylic acid preferential RNase, whereas RNase NT is the enzyme with a broad base specificity. The crystal structural analysis of RNase NW in complex with 5′-GMP revealed that the guanine ring of 5′-GMP predominantly binds B2 site and identified Gln12, Tyr17, Thr78, Leu79, and Phe89 as building blocks of the B2 site (*15*). Since the amino acid residues involved in the 5′-GMP interaction in RNase NW are conserved as Gln12, Tyr17, Ser78, Leu79, and Phe89 in RNase NT, they could be expected to participate in base bindings. Indeed, the present study shows that the base moieties of 5′-GMP and 5′-AMP bound at the B2 site in RNase NT are recognized in a manner similar to that of 5′-GMP in the complex RNase NW-5′-GMP, though the adenine base of 5′-AMP adopts a different orientation from the guanine base of 5′-GMP. Thus, the glycosyl bond of 5′-AMP is an *anti* conformation, while that of 5′-GMP is a *syn* conformation. Despite of a distinct orientation, the adenine and guanine bases are recognized by amino acids (Gln12, Tyr17, Ser78, Leu79, and Phe89) composed of the B2 site in RNase NT. Similarly, although base moieties of 5′-GMP and 5′-AMP bound the B1 site adopt a different orientation, both bases are recognized by amino acids (Trp42, Asn44, and Trp50) composed of the B1 site

in RNase NT. Furthermore, a docking study with 5′-GMP, 5′-AMP, or diribonucleoside monophosphates, such as GpG, or ApA, indicated that guanine and adenine bases lie on B1 and B2 sites in a manner approximately identical to those observed in the crystal structures of the complexes, though adenine base bound at the B1 shows two distinct conformations: one is an *anti* conformation as observed in the crystal structure, while the other is a *syn* conformation (Nakashima *et al*., unpublished results). Hence, although we can not exclude the possibility that the binding modes observed in the crystal structures would be inhibitory modes, the orientation of the adenine and guanine bases observed at the B1 and B2 sites in RNase NT might be an adequate binding mode for hydrolysis.

In contrast to 5′-AMP and 5′-GMP, no binding of 2′-UMP was observed at the B2 site. Our previous structural comparison showed that substitution of Asn71 in the uridylic acid preferential RNase MC1 with the corresponding amino acids Thr or Ser in the guanylic acid preferential RNases cause an enlargement of the B2 site, which make it feasible to insert a guanine base into the B2 site (*16*). It could be assumed that the large size of the B2 site in RNase NT may not allow the uracil base of 2′-UMP to interact with amino acid residues composed of the B2 site.

It is generally known that RNases, including RNases belonging to the RNase A and RNase T1 families, degrade the phosphodiester bond, primarily recognizing the base located at the 5′-side of the scissile bond, though the dependency of the catalytic rate on the nature of the nucleotide at the 3′-side of scissile bond is known to be a general feature. Thus, base specificity is usually attributable to the nature of the interaction of B1 site with the base located at the 5′-terminal end. This is the case for the representative RNase T2 family enzyme RNase Rh, where Trp49, Asp51, and Tyr57 are assigned as building blocks to constitute the B1 site (*4*, *5*). In this context, the specificities of plant RNases, such as RNase NW and RNase MC1, set by the bases at the 3′-terminal side of the scissile bond are distinct from other RNases. It is speculated that RNase NW and RNase MC1 might have diverged from an archetype of fungal non–base-specific RNase, acquiring a subsite structure capable to bind to the bases at the 3′-side of the scissile bond. The present study on RNase NT reveals that 5′-GMP and 5′-AMP bind not only to B2 site but also to B1 site, and 2′-UMP predominantly binds to B1 site in RNase NT; Trp42, Asn44, and Trp50 are found to be involved in the interaction with base moieties at the B1 site. Comparing these amino acids with the corresponding residues in RNase NW, Trp50 in RNase NT is substituted with Tyr50 in RNase NW, though Trp42 and Asn44 are conserved in the two molecules. It could be assumed that a sandwich-like interaction provided by indole rings of two Trp residues (Trp42 and Trp50) in RNase NT may form a binding site with higher affinity than that by a phenolic side chain (Tyr50) and indole ring side chain (Trp42) in RNase NW. It could be speculated that replacement of Tyr50 in RNase NW with Trp in RNase NT results in formation of a more hydrophobic pocket, thereby making it possible to dock adenine, guanine, and uracil bases into the B1 site in RNase NT. The characteristic feature of the B1 site in RNase NT may partly explain for a broad substrate specificity of RNase NT.

We thank Drs. M. Kawamoto and H. Sakai of the RIKEN Harima Institute for help with data collection using synchrotron radiation at beamlines. This work was supported in part by a grant from the National Project on Protein Structural and Functional Analyses, and by a Grant-in-Aid for Scientific Research from the Ministry of Education, Science, Technology, Sports and Culture of Japan.

## REFERENCES

1. Irie, M. (1999) Structure-function relationships of acid ribonucleases: Lysosomal, vacuolar, and periplasmic enzymes. *Pharmacol. Ther.* **81**, 77–89
2. Horiuchi, H., Yanai, K., Tagagi, M., Yano, K., Wakabayashi, E., Sanda, A., Mine, S., Ohgi, K., and Irie, M. (1988) Primary structure of a base non-specific ribonuclease from *Rhizopus niveus*. *J. Biochem.* **103**, 408–418
3. Tomoyeda, M., Eto, Y., and Yoshino, T. (1969) Studies on ribonuclease produced by *Rhizopus* sp, I. Crystallization and some properties of the ribonuclease. *Arch. Biochem. Biophys.* **131**, 191–202
4. Ohgi, K., Horiuchi, H., Iwama, M., Watanabe, H., Takagi, M., and Irie, M. (1992) Evidence that three histidine residues of a base non-specific and adenylic acid preferential ribonuclease from *Rhizopus niveus* are involved in the catalytic function. *J. Biochem.* **112**, 132–138
5. Irie, M., Ohgi, K., Iwama, M., Koizumi, M., Sasayama, E., Harada, K., Yano, Y., Udagawa, J., and Kawasaki, M. (1997) Role of histidine 46 in the hydrolysis and the reverse transphosphorylation reaction of RNase Rh from *Rhizopus niveus*. *J. Biochem.* **121**, 849–853
6. Kurihara, H., Nonaka, T., Mitsui, Y., Ohgi, K., Irie, M., and Nakamura, KT. (1996) The crystal structure of ribonuclease Rh from *Rhizopus niveus* at 2.0 Å resolution. *J. Mol. Biol.* **255**, 310–320
7. Nakamura, T., Ishikawa, N., Hamashima, M., Kurihara, H., Nonaka, T., Mitshui, Y., Ohgi, K., and Irie, M. (1993) Protein nucleic acid recognition in ribonuclease Rh-2′-adenylic acid complex. In: *The 3rd International Meeting on Ribonuclease, Chemistry, Biology, Biotechnology*, Capri, p. 5
8. McClure, B.A., Haring, V., Ebert, P.R., Anderson, M.A., Simpson, R.J., Sakiyama, F., and Clarke, A.E. (1989) Style self-incompatibility gene products of *Nicotiana alata* are ribonucleases. *Nature* **342**, 955–957
9. Green, P.J. (1994) The ribonuclease of higher plants. *Annu. Rev. Plant Physiol. Plant Mol. Biol.* **45**, 421–445
10. Abel, S. and Glund, K. (1987) Ribonuclease in plant vacuoles: purification and molecular properties of the enzyme from cultured tomato cells. *Planta* **172**, 71–78
11. Nurnberger, T., Abel, S., Jost, W., and Glund, K. (1990) Induction of an extracellular ribonuclease in cultured tomato cells upon phosphate starvation. *Plant Physiol.* **92**, 970–976
12. Irie, M., Watanabe, H., Ohgi, K., Minami, Y., Yamada, H., and Funatsu, G.. (1993) Base specificity of two plant seed ribonucleases from *Momordica charantia* and Luffa cylindrical. *Biosci. Biotechnol. Biochem.* **57**, 497–498
13. Nakagawa, A., Tanaka, I., Sakai, R., Nakashima, T., Funatsu, G., and Kimura, M. (1999) Crystal structure of a ribonuclease from the seeds of bitter gourd (*Momordica charantia*) at 1.75 Å resolution. *Biochem. Biophys. Acta* **1433**, 253–260
14. Suzuki, A., Yao, M., Tanaka, I., Numata, T., Kikukawa, S., Yamasaki, N., and Kimura, M. (2000) Crystal structures of the ribonuclease MC1 from bitter gourd seeds, complexed with 2′-UMP or 3′-UMP, reveal structural basis for uridine specificity. *Biochem. Biophys. Res. Commun.* **275**, 572–576

15. Kawano, S., Kakuta, Y., and Kimura, M. (2002) Guanine binding site of the *Nicotiana glutinosa* ribonuclease NW revealed by X-ray crystallography. *Biochemistry* **41**, 15195–15202
16. Numata, T., Suzuki, A., Yao, M., Tanaka, I., and Kimura, M. (2001) Amino acid residues in rebonuclease MC1 from bitter gourd seeds which are essential for uridine specificity. *Biochemistry* **40**, 524–530
17. Kurata, N., Kariu, T., Kawano, S., and Kimura, M. (2002) Molecular cloning of cDNAs encoding ribonuclease-related proteins in *Nicotiana glutinosa* leaves, as induced in response to wounding or to TMV-infection. *Biosci. Biotechnol. Biochem.* **66**, 391–397
18. Hino, M., Kawano, S., and Kimura, M. (2002) Expression of *Nicotiana glutinosa* ribonucleases in *Escherichia coli*. *Biosci. Biotechnol. Biochem.* **66**, 910–912
19. Otwinowski, Z. and Minor, W. (1997) Processing of x-ray diffraction data collected in oscillation mode. In *Methods in Enzymology* Vol. 276: *Macromolecular Crystallography*, part A (Carter, C.W., Jr. and Sweet, R.M., eds.) pp. 307–326, Academic Press, New York
20. Brunger, A.T., Adams, P.D., Clore, G.M., Delano, W.L., Gros, P., Grosse-Kuntleve, R.W., Jiang, J. S., Kuszewski, J., Nilges, M., Pannu, N.S., Read, R.J., Rice, L.M., Simonson, T., and Warren, G.L. (1998) Crystallography and NMR system (CNS): a new software system for macromolecular structure determination. *Acta Crystallogr.* **D54**, 905–921
21. Jones, T.A., Zou, J.Y., Cowan, S.W., and Kjeldgaard, M. (1991) Improved methods for building protein models in electron density maps and the location of errors in these models. *Acta Cryst.* **A47**, 110–119
22. Laskowski, R.A., MacArthur, M.W., Moss, D.S., and Thornton, J.M. (1993) PROCHECK: a program to check the stereochemical quality of protein structures. *J. Appl. Crystallogr.* **26**, 283–291
23. Allewell, N.M. and Wyckoff, H.W. (1971) Crystallographic analysis of the interaction of cuypric ion with ribonuclease S. *J Biol Chem.* **246**, 4657–4663